Two-Color Vector Solitons In Nonlocal Media

Alessandro Alberucci, Marco Peccianti, and Gaetano Assanto

NooEL—Nonlinear Optics and OptoElectronics Laboratory, Department of Electronic Engineering and CNISM, University "Roma Tre," Via della Vasca Navale, 84-00146 Rome, Italy

Andriy Dyadyusha and Malgosia Kaczmarek

School of Physics and Astronomy, University of Southampton, Southampton, United Kingdom

(Received 13 March 2006; published 12 October 2006)

We investigate the interaction between two beams differing in wavelength and the properties of dual-frequency spatial solitons in nonlocal birefringent reorientational media. We report the first experimental observations of anisotropic nonlocal vector solitons in unbiased nematic liquid crystals. Model and simulations, based on the paraxiality along the Poynting vectors, include joint walk-off and breathing.

DOI: 10.1103/PhysRevLett.97.153903 PACS numbers: 05.45.Yv, 42.65.−k, 77.84.Nh

Spatial optical solitons have been widely investigated, mainly because of their potentials in all-optical information processing [1–3]. Spatial solitons in 2 + 1 dimensions have been studied in several materials, from photorefractives [4,5] to $\chi^{(2)}$ crystals [6,7], from liquids [8] to liquid crystals [9,10]. Recently, anisotropic spatial solitons and their angular walk-off and steering have been observed in specifically designed liquid crystalline cells [11].

The simplest vector solitons (VS) are known as shape-preserving, self-localized solutions of coupled nonlinear evolution equations [1]. Among them, Manakov spatial solitons [12] can be derived by the inverse scattering technique and were first observed in AlGaAs with orthogonally polarized collinear beams interacting incoherently [13]. Two-wavelength vector solitons in Kerr media were predicted by De La Fuente and coworkers [14], whereas VS consisting of bright and dark solitons were reported by Shalaby and Barthelemy [15]. Quadratic solitons belong to the class of VS because they encompass the parametric interaction of waves at different wavelengths [6,7,16]. The resulting self-guided beams, in general, have energy flows along directions depending on relative powers and birefringence [7]. In photorefractives, VS were demonstrated in various forms, ranging from incoherent VS [17] to VS with bright and dark solitary components [18], soliton dipoles [19] and multimode solitons [17,20]. The rich VS phenomenology is grasped by the term *molecule soliton* [21].

In this Letter, we investigate for the first time a novel class of VS, namely, two-color spatial solitons in a highly nonlocal and anisotropic Kerr-like medium. While each color component experiences a different degree of birefringence and walk-off because of dispersion, the generated nonlocal vector soliton is a self-localized wave with a single Poynting vector and a complex breathing behavior. We carry out the analysis at the two frequencies adopting the paraxial approximation, i.e., modeling wave propagation along each Poynting vector [11,22] and assuming an incoherent mutual interaction owing to nonlocality in both time and space. In order to address the most general case of an optically tunable anisotropy, we consider the additional effect of (nonlinear) self-focusing on (linear) walk-off and refer to a reorientational response, such as in nematic liquid crystals (NLC). We verify our main findings in the limit of single walk-off using NLC in a highly nonlocal configuration.

We consider the cell geometry sketched in Fig. 1, with optic axis $\hat{n}$ in the plane yz at an angle ϕ with respect to z. Two Gaussian beams of distinct wavelengths (namely λ_1 and λ_2), polarized as extraordinary waves, are launched in $z = 0$ with wave vectors $\mathbf{k}_j$ $(j = 1, 2)$ in the plane yz. Each (individual) beam would normally undergo walk-off at an angle $\delta = \arctan(\varepsilon_a \sin(2\vartheta)/[\varepsilon_a + \varepsilon_a \cos(2\vartheta) + 2\varepsilon_\perp)]$, with ϑ the angle between $\mathbf{k}_j$ and the molecular director $\hat{n}$; $\varepsilon_\perp$ and $\varepsilon_\parallel$ the relative dielectric constants perpendicular and parallel to the optic axis, respectively; and $\varepsilon_a = \varepsilon_\parallel - \varepsilon_\perp$ the optical anisotropy. The dielectric tensor $\bar{\bar{\varepsilon}}$ elements can be expressed as $\varepsilon_{ij} = \varepsilon_\perp \delta_{ij} + \varepsilon_a(\hat{i} \cdot \hat{n})(\hat{j} \cdot \hat{n})$, with δ_{ij} the Kronecker delta and $\hat{i}, \hat{j}$ spanning the axes versors. Since all material constants are λ dependent, δ differs at the two wavelengths. To avoid additional walk-off along x,

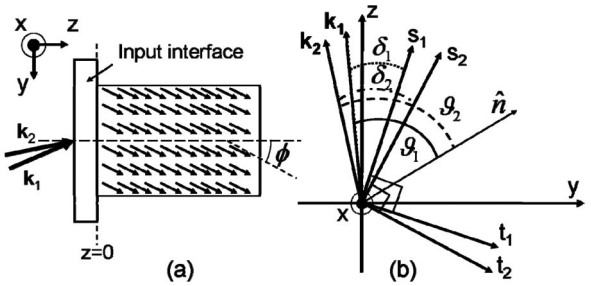

FIG. 1. (a) Schematic top view of the cell. Small arrows illustrate the director distribution in the absence of external perturbation (voltage and/or light). The large arrows represent the input wave vectors. (b) Sketch of propagation vectors $\mathbf{k}_j$ with respect to the optic axis $\hat{n}$. Rotated reference frames xt_1s_1 and xt_2s_2 are indicated, as well.

we look at the case with no external bias [11]; hence the equation governing the reorientation ϑ for electric fields in the principal plane yz is

$$K\nabla^2\vartheta_j + \frac{\varepsilon_0\varepsilon_{a1}}{4}|A_1|^2\sin[2(\vartheta_1-\delta_1)] + \frac{\varepsilon_0\varepsilon_{a2}}{4}|A_2|^2\sin[2(\vartheta_2-\delta_2)] = 0, \quad (1)$$

with the subscript j referring to the two wavelengths λ_j $(j=1,2)$, ε_{aj} the anisotropies, A_j the field envelopes, $\nabla^2\vartheta_1 = \nabla^2\vartheta_2$ for any set of propagation vectors $\mathbf{k}_j$, ϑ_j the angle between the optic axis $\hat{n}$ and $\mathbf{k}_j$, and K the elastic constant (single constant approximation [23]). The latter quantifies the elastic response which, in conjunction with the boundary conditions, rules nonlocality in space. In Eq. (1), mixing terms which involve both fields were neglected due to nonlocality in time, i.e., because of the incoherent nature of the interaction [24].

After rotating the initial xyz reference system by an angle δ_j around the x axis, the evolution equations in the new coordinate systems $x_jt_js_j$ are

$$2ik_{0j}n_{ej}\cos\delta_j\frac{\partial A_j}{\partial s_j} + D_{tj}\frac{\partial^2 A_j}{\partial t_j^2} + D_{xj}\frac{\partial^2 A_j}{\partial x_j^2} + k_{0j}^2\delta\varepsilon_{ttj}A_j = 0 \qquad (j=1,2), \quad (2)$$

with D_{xj} and D_{tj} the diffraction coefficients along x_j and t_j, respectively; $k_{0j} = 2\pi/\lambda_j$; $n_{ej}(\vartheta_{0j})$ the unperturbed extraordinary (e-)wave indices (in the absence of optical reorientation) being ϑ_{0j} the values of ϑ_j in the linear limit; $\delta\varepsilon_{ttj}$ the all-optical perturbation induced on the $\hat{t}\hat{t}$ element of the dielectric tensor $\bar{\bar{\varepsilon}}_j$, i.e., $\delta\varepsilon_{ttj} = \varepsilon_{aj}[\sin^2(\vartheta_j-\delta_j) - \sin^2(\vartheta_{0j}-\delta_j)]$ [see Fig. 1(b)]. Noteworthy, at this order of approximation, the fields are linearly polarized along t_j, consistently with the hypothesis used in deriving Eq. (1). Since each $\delta\varepsilon_{ttj}$ depends nonlocally on field intensities through Eq. (1), Eq. (2) is an incoherently coupled nonlocal equation encompassing a Kerr-like nonlinearity.

Let us now consider collinear beams with propagation vectors parallel to $\hat{z}$, hence $\vartheta_1 = \vartheta_2 = \vartheta$. Based on walk-off (we take $\delta_2 > \delta_1$) and mutual attraction [24], we expect the corresponding trajectories to oscillate in propagation, with a mean angular direction depending on the relative power balance. We set $\vartheta = \vartheta_0 + \Psi$, with $\Psi \ll \vartheta_0$ the optically induced perturbation [10]. Defining $\beta = (\delta_2 - \delta_1)/2$ and rewriting Eq. (1) in the frame xts obtained by rotating xyz of an angle $\delta_1 + \beta$ around x, linearizing the equation about ϑ_0 and assuming radial symmetry as well as negligible second order derivatives along s, the perturbation can be expressed as

$$\Psi = \Psi_0 + \Psi_2^{(1)}\{x^2 + [t - \bar{t}_1(s)]^2\} + \Psi_2^{(2)}\{x^2 + [t - \bar{t}_2(s)]^2\}, \quad (3)$$

where Ψ_0 is the maximum perturbation and $\Psi_2^{(j)} = -(\varepsilon_0\varepsilon_{aj}/16K)|A_j|^2_{x=0,t=0}\sin[2(\vartheta_0-\delta_j)]$ $(j=1,2)$. $\bar{t}_j(s)$ is the average trajectory of the jth beam in the plane st, i.e., $\bar{t}_j(s) = \iint |A_j(x,t,s)|^2 t\,dx\,dt$. By linearizing Eq. (2) around ϑ_0 and using Eq. (3), we obtain

$$2ik_{0j}n_{ej}\cos\delta_j\frac{\partial A_j}{\partial s_j} + D_j\frac{\partial^2 A_j}{\partial t_j^2} + D_j\frac{\partial^2 A_j}{\partial x_j^2} + k_{0j}^2\varepsilon_{aj}\sin[2(\vartheta_0-\delta_j)]\{\Psi_0 + \Psi_2^{(1)}[x_j^2 + (t_j - \bar{t}_1)^2] + \Psi_2^{(2)}[x_j^2 + (t_j - \bar{t}_2)^2]\}A_j = 0 \qquad (j=1,2), \quad (4)$$

with $D_{xj} = D_{tj} = D_j$ due to radial symmetry. Letting $\hbar = 1$, $m_j = (k_{0j}n_{ej}\cos\delta_j)/D_j$, $V_{\mathrm{eq}}^j = -\gamma_j\Psi$, and $\gamma_j = \{k_{0j}^2\varepsilon_{aj}\sin[2(\vartheta_0-\delta_j)]\}/(2m_jD_j)$, it is straightforward to recognize that (4) are of the form $i\hbar\partial A_j/\partial s_j + (\hbar^2/2m)\nabla^2 A_j - V_{\mathrm{eq}}^j = 0$, i.e., Schrödinger equations able to support stable spatial solitons [11,25]. In the limit of self-confinement, i.e., with $\Psi_2^{(j)}$ independent from s, after applying the Ehrenfest's theorem, the average beam trajectories in the frame $x_1t_1s_1$ are (with no variations in x, as expected) as follows:

$$\bar{t}_1 = -\left(-\frac{1}{\alpha^2} + \frac{m_2}{2\gamma_2\Psi_2^{(1)}}\right)\frac{2\tan(2\beta)\gamma_2\Psi_2^{(1)}}{\alpha m_2}\sin(\alpha s) + \tan(2\beta)\left(1 - \frac{2\gamma_2\Psi_2^{(1)}}{\alpha^2 m_2}\right)s,$$

$$\bar{t}_2 = \frac{1}{\alpha^2}\frac{2\tan(2\beta)\gamma_2\Psi_2^{(1)}}{\alpha m_2}\sin(\alpha s) + \tan(2\beta)\left(1 - \frac{2\gamma_2\Psi_2^{(1)}}{\alpha^2 m_2}\right)s,$$

where we defined $\alpha = -2(m_1\gamma_2\Psi_2^{(1)} + m_2\gamma_1\Psi_2^{(2)})/(m_1m_2)$. Therefore, the two wavelength components oscillate around a straight line lying in the plane yz at an angle Δ with z, being

$$\Delta = \arctan\left[\tan(2\beta)\left(1 - \frac{m_1\gamma_2\Psi_2^{(1)}}{m_1\gamma_2\Psi_2^{(1)} + m_2\gamma_1\Psi_2^{(2)}}\right)\right] + \delta_1, \quad (5)$$

i.e., when the combined excitations induce self-confinement, the VS has energy flow along a direction established by the (two) power components according to Eq. (5).

Having ascertained that a VS is indeed a self-localized solution with a well-defined, power-dependent walk-off, it is even more intriguing to focus on the breathing features of this VS by introducing an input wave front tilt on the second beam, in order to make $\hat{s}_1$ and $\hat{s}_2$ parallel to one another and rewrite Eq. (2) in a common reference. Since the electric fields are parallel, their angle with the optic axis $\hat{n}$ is the same, i.e., $\vartheta_1 - \delta_1 = \vartheta_2 - \delta_2$, with two distinct ϑ_0, namely $\vartheta_{01} = \phi$ and ϑ_{02}. Therefore, we have to deal with the partial differential equations system consisting of Eq. (1) (with $\partial^2/\partial s^2 = 0$) and Eq. (4), with Eq. (3) and $\bar{t}_1(s) = \bar{t}_2(s) = 0$ (the Poynting vectors are collinear and no mutual attraction takes place). The

coupled Schrödinger equations [Eq. (4)]—with parabolic potentials nonlinearly depending on the beam amplitudes—describe an induced waveguide with index distribution longitudinally varying through cross-phase modulation (XPM): consequently, eigenmodes and eigenvalues change continuously with s, originating different breathing at the two wavelengths and, in general, a nonperiodic propagating behavior for the nonlocal VS.

In the experiments, we employed an NLC cell with two parallel glass slides, their interfaces polymer coated and rubbed at $\pi/6$ with respect to z. The cell thickness was 100 μm and contained the nematic liquid crystal E7. Consequently, in the absence of any perturbation, the NLC director was homogeneously aligned in yz at $\pi/6$ with respect to z. An input interface parallel to plane xy (see Fig. 1) prevented lenslike effects and depolarization of the input waves. We injected two extraordinarily polarized Gaussian beams of wavelengths of 632.8 (red) and 1064 nm (NIR), respectively, and acquired images of their intensity distributions in the plane yz by means of a CCD camera and a microscope, collecting the light scattered out of the plane. We monitored light evolution at both wavelengths, but in order to prevent chromatic effects, we filtered and reproduced only images of the visible component at 632.8 nm. The optics were arranged as to launch both beams with Rayleigh lengths equal to 60 μm, i.e., input waists of 2.8 and 3.7 μm for red and NIR, respectively. By adjusting the input phase-front tilt of the red, we carried out experiments with collinear Poynting vectors along z. We firstly investigated their linear behavior, i.e., when each beam diffracted either in the absence of the second one or in the presence of negligible XPM, then we launched both components to exploit XPM and generate a VS. We reproduced the photographs [Fig. 2] after color (gray) coding and a rotation by δ in order to correct for the walk-off, i.e., to show light propagation versus s rather than z. Figure 2(a) is the ts evolution of a low-power (0.1 mW) red beam colaunched with a 1.2 mW NIR beam; the latter is unable to self-localize and both components diffract. Similarly, Fig. 2(b) displays a 0.4 mW red beam propagating and diffracting in the absence of NIR. When 1.2 mW NIR and 0.4 mW red beams are collinearly injected together as in Fig. 2(c), the nonlinear response is enhanced through incoherent XPM and supports a self-localized wave, i.e., a two-color vector soliton. To compare our data with numerical simulations, we set $\phi = \pi/6$, assumed the propagation vector $\mathbf{k}_2$ (red beam) to be tilted in the plane yz to make $\hat{s}_1$ and $\hat{s}_2$ collinear, and used a standard split-step approach with a Crank-Nicolson scheme to solve the propagation equations. We took $K = 12 \times 10^{-12} N$ and the material parameters of E7 [26]. The white contour lines in Fig. 2 display the simulated behavior. Consistently with the actual experimental limitations (the use of a nonachromatic lens, wavelength dependent Fresnel reflections and scattering, the presence of a nonhomogeneous NLC transition layer in $0 \leq z < 100$ μm), we included a phase-front curvature for the input beams

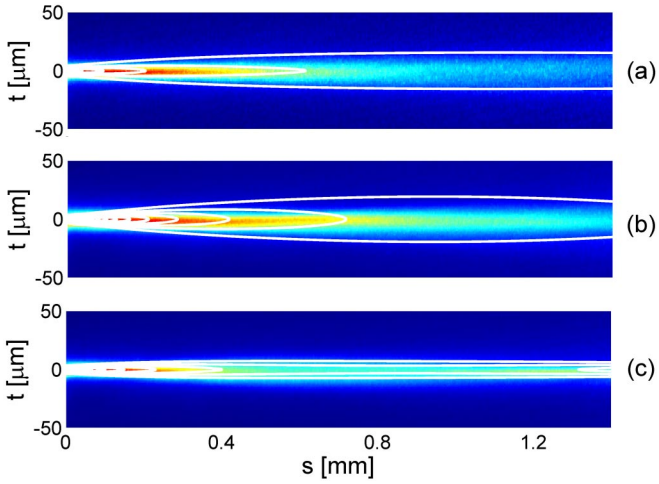

FIG. 2 (color online). Acquired intensity profiles for red light in the plane ts (i.e., after a rotation by δ). Contour maps of the calculated intensity distributions are superimposed (white lines) to the experimental data. (a) A weak 0.1 mW red beam is colaunched with a 1.2 mW NIR beam; (b) a 0.4 mW red beam is injected in the absence of NIR; (c) 0.4 mW red and 1.2 mW NIR beams are colaunched and generate a vector soliton. In the simulations, we took effective input coupling efficiency of 40% and 50% for red and NIR and initial beam curvatures of radius -130 μm (waist in $z = -40$ μm), respectively.

and distinct effective incoupling factors at the two wavelengths.

To pursue a systematic study of these multicomponent beams, we varied both red and NIR input powers P_R and P_{NIR}, respectively, while keeping the launch conditions (Rayleigh lengths, tilt, polarization) fixed. Figures 3(a), 3(c), and 3(e) show the yz evolution of a red beam of fixed power as the NIR excitation is increased; clearly, the red becomes more and more confined versus P_{NIR}, as expected

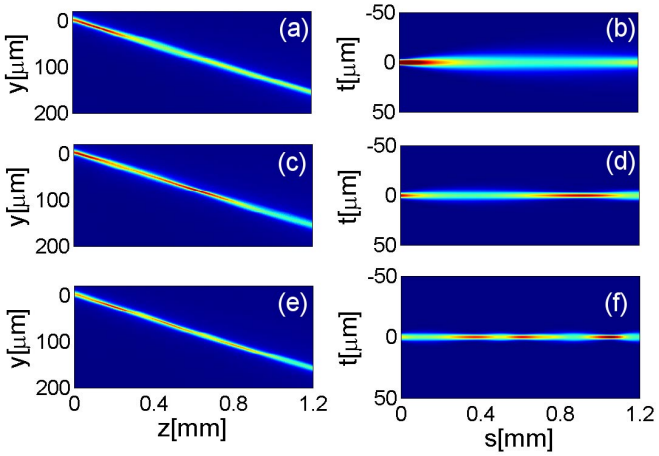

FIG. 3 (color online). Left: acquired intensities profiles at 632.8 nm in the plane yz. Intensity levels are normalized to scattering. Right: corresponding computed intensities in the plane st. Input power P_R at 632.8 nm is 1.6 mW, while NIR powers are $P_{NIR} = 0$ (a),(b), 0.7 (c),(d), and 2.4 mW (e),(f), respectively. Incoupling parameters are as in Fig. 2.

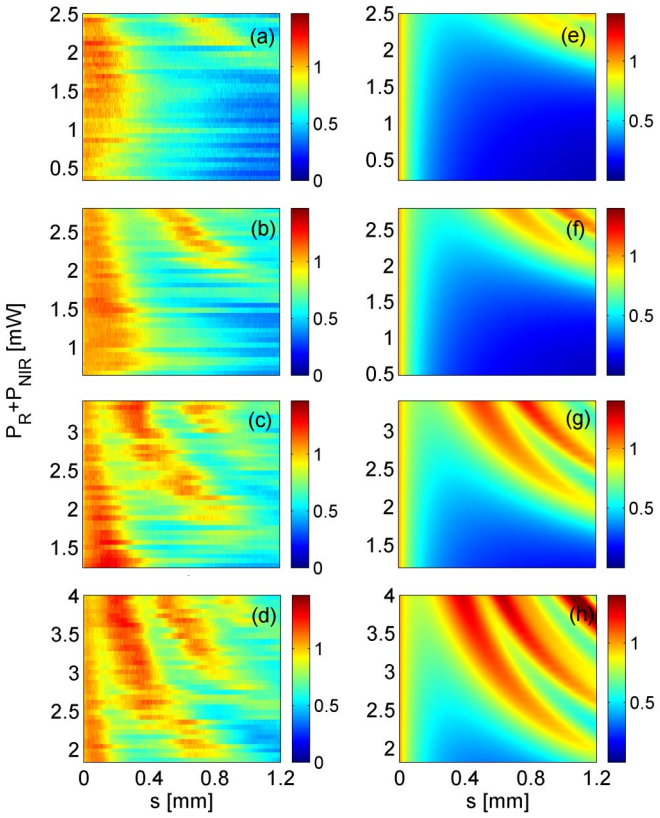

FIG. 4 (color online). Red peak intensity $I_R(s)$ in the observation plane st (right axes) versus s and total excitation $P_R + P_{NIR}$ (left axes) for a fixed P_R. (a)–(d): measured data; (e)–(h): calculated data (after integration along x) assuming coupling parameters as in Fig. 2. P_R is 0.1 (a),(e), 0.4 (b),(f), 1.0 (c),(g), and 1.6 mW (d),(h), respectively. All data are normalized to the value in $s = 0$.

on the basis of XPM [Eq. (1)]. A similar behavior is verified for the NIR and, as predicted, both components propagate along the same Poynting direction s. Once again, measured and calculated data [in the plane ts, Figs. 3(b), 3(d), and 3(f)] are in excellent agreement.

Finally, Figs. 4(a)–4(d) show color-coded maps of the measured peak intensity (normalized to scattering losses) of the red component versus s (horizontal axis) and total excitation $P_R + P_{NIR}$ (vertical axis) for a fixed input power P_R at 632.8 nm. It is apparent that the characteristic breathing [10] of the nonlocal vector soliton is nonperiodic and changes with total excitation, being more sensitive to the red component (i.e., a similar behavior occurs at lower total powers if P_R is higher). This is primarily due to the larger anisotropy at 632.8 nm, i.e., a greater amount of energy coupled with the medium through reorientation [see Eq. (1)], and a deeper refractive well for a given director distribution [Eq. (2)]. The simulations, plotted in Fig. 4(e)–4(h) for the peak intensity after integration across the thickness x and normalization to the input power at 632.8 nm, display the same trend: for a fixed total power P, a larger P_R makes the soliton more confined and accelerates the breathing oscillations versus s, in good agreement with the experimental results. The departure between acquired (a through d) and calculated maps (e through h) in Fig. 4 can be ascribed to scattering losses as well as beam aberrations due to the distorted director distribution at the input interface, both effects neglected in the simulations.

In conclusion, we have demonstrated for the first time anisotropic vector solitons in nonlocal birefringent media exhibiting a reorientational nonlinearity. Two extraordinarily polarized beams of different wavelengths—hence walk-off—can nonlinearly couple in an incoherent fashion and combine into a vector soliton with a given Poynting vector and an aperiodic breathing determined by dispersion, birefringence, and relative excitations.

[1] Y. S. Kivshar and G. P. Agrawal, *Optical Solitons* (Academic Press, San Diego, 2003).
[2] S. Trillo and W. Torruellas, *Spatial Solitons* (Springer-Verlag, Berlin, 2001).
[3] G. I. Stegeman and M. Segev, Science **286**, 1518 (1999).
[4] W. Krolikowsky, B. Luther-Davies, and C. Denz, IEEE J. Quantum Electron. **39**, 3 (2003).
[5] M. Segev, B. Crosignani, A. Yariv, and B. Fischer, Phys. Rev. Lett. **68**, 923 (1992).
[6] W. E. Torruellas *et al.*, Phys. Rev. Lett. **74**, 5036 (1995).
[7] W. E. Torruellas *et al.*, Appl. Phys. Lett. **68**, 1449 (1996).
[8] A. Barthelemy, S. Maneuf, and C. Froehly, Opt. Commun. **55**, 201 (1985).
[9] G. Assanto and M. Peccianti, IEEE J. Quantum Electron. **39**, 13 (2003).
[10] C. Conti, M. Peccianti, and G. Assanto, Phys. Rev. Lett. **92**, 113902 (2004).
[11] M. Peccianti *et al.*, Nature (London) **432**, 733 (2004).
[12] S. V. Manakov, Sov. Phys. JETP **38**, 248 (1974).
[13] J. U. Kang, G. I. Stegeman, J. S. Aitchison, and N. Akhmediev, Phys. Rev. Lett. **76**, 3699 (1996).
[14] R. De La Fuente and A. Barthelemy, Opt. Commun. **88**, 419 (1992).
[15] M. Shalaby and A. J. Barthelemy, IEEE J. Quantum Electron. **28**, 2736 (1992).
[16] G. Assanto and G. I. Stegeman, Opt. Express **10**, 388 (2002).
[17] M. Mitchell, M. Segev, and D. N. Christodoulides, Phys. Rev. Lett. **80**, 4657 (1998).
[18] D. N. Christodoulides *et al.*, Appl. Phys. Lett. **68**, 1763 (1996).
[19] W. Krolikowski *et al.*, Phys. Rev. Lett. **85**, 1424 (2000).
[20] T. Carmon *et al.*, Opt. Lett. **25**, 1113 (2000).
[21] V. M. Perez-Garcia and V. Vekslerchik, Phys. Rev. E **67**, 061804 (2003).
[22] C. Conti, M. Peccianti, and G. Assanto, Phys. Rev. E **72**, 066614 (2005).
[23] P. G. De Gennes and J. Prost, *The Physics of Liquid Crystals* (Oxford Science, New York, 1993).
[24] M. Peccianti, K. A. Brzdakiewicz, and G. Assanto, Opt. Lett. **27**, 1460 (2002).
[25] C. Conti, M. Peccianti, and G. Assanto, Phys. Rev. Lett. **91**, 073901 (2003).
[26] *CRC Handbook of Laser Science and Technology*, edited by M. J. Weber (CRC Press, Boca Raton, FL, 1995).